Pressure-Induced Phase Transformations, Electronic Properties and Intermediate Phases of Chromium Dioxide

H. Öztürk[a] and C. Kürkçü[b,*]

[a]Department of Physics, Ahi Evran University, Kırşehir, 40100, Turkey

[b]Department of Electronics and Automation, Ahi Evran University, Kırşehir, 40100, Turkey

(Received October 29, 2017; revised version March 11, 2019; in final form July 18, 2019)

We study pressure-induced phase transformations of chromium dioxide (CrO_2) using constant pressure *ab initio* simulations. A first-order phase transformation from the rutile-type structure to the $CaCl_2$-type structure is successfully observed at 220 GPa. Simulations reveal that this transformation proceeds via two intermediate phases within $P\bar{4}2_1m$ and $P2_12_12$ symmetries. Another phase transformation from this structure to the orthorhombic structure with space group $Cmc2_1$ occurs at 440 GPa. This phase transformation also proceeds via two intermediate phases within $P2_1/c$ and $P2_1$ symmetries. We also study these phase transformations of CrO_2 by undertaking the enthalpy calculations. We find that the phase transformation from the rutile-type structure to the $CaCl_2$-type structure occurs around 15 GPa which is in good agreement with the experiments. Also, the phase transformation from $CaCl_2$-type to the orthorhombic structure with space group $Cmc2_1$ is found at 105 GPa. Additionally, we predict band gaps from electronic structure calculations for obtained phases of CrO_2

DOI: 10.12693/APhysPolA.136.26

PACS/topics: chromium dioxide, high pressure, phase transformation, intermediate phase

1. Introduction

Chromium dioxide (CrO_2) has attracted specific interest as a compound possessing near 100% spin polarization at the Fermi level. Its half-metallic performance leads to relatively low electrical resistivity for an oxide. It is also ferromagnetic at room temperature relative to the other half-metal candidates. These properties and wide availability of CrO_2 make this material technologically and scientifically noteworthy and a perfect substance for developing spintronic devices [1–11].

This material is regarded as a perfect candidate for enhancing spintronic devices, tunneling magnetoresistance devices, magnetic heads, magnetic random access memories, and magnetic field sensors. Due to the uniaxial crystal structure, CrO_2 is estimated to have a great magnetic anisotropy which makes it a preferable material for magneto-optical recording [3, 12–21].

CrO_2 crystallizes in a tetragonal rutile-type structure with space group $P4_2/mnm$ at ambient conditions like TiO_2, MnO_2, RuO_2, SnO_2, GeO_2, etc. Among these rutile-type dioxides, CrO_2 has exceptional meaning because CrO_2 is the only half-metallic ferromagnet. A phase transformation from the tetragonal rutile-type to the $CaCl_2$-type structure is observed by Maddox et al. [12] at 12 ± 3 GPa.

We have also found this phase transformation at about 15 GPa by *ab initio* calculations in good agreement with their study. We also suggest that this orthorhombic structure with space group $Pnnm$ of CrO_2 proceeds through two intermediate phases with space groups $P\bar{4}2_1m$ and $P2_12_12$, expressed as CrO_2-(a) and CrO_2-(b), respectively. To our knowledge, these intermediary phases of this material have not been found in any earlier studies. Additionally, we have observed a new phase transformation of this material from the $CaCl_2$-type structure to an orthorhombic structure with space group $Cmc2_1$ at about 105 GPa. This orthorhombic structure also proceeds through two intermediate phases with space group $P2_1/c$ and $P2_1$, expressed as CrO_2-(c) and CrO_2-(d), respectively. This orthorhombic structure has not been recognized for CrO_2 before, to the best of our knowledge.

2. Computational details

The calculations in the present work were carried out in the frame of density-functional theory (DFT) with the *ab initio* program SIESTA [22]. Local density approximation (LDA) using the Ceperley–Alder functional [23] was used for the exchange-correlation energy. Double-ξ plus polarized basis sets were employed and a uniform mesh with a plane wave cut-off of 200 Ry was used. A chosen simulation cell consists of 96 atoms with periodic boundary conditions. We employed Γ-point sampling for the Brillouin zone integration. To get optimized lattice vectors and atomic positions, the stress tolerance and maximum atomic force were taken less than 0.5 GPa and smaller than 0.01 eV Å^{-1}, respectively. Firstly, the system was equilibrated at zero pressure, and after that the pressure was gradually increased by an increment of 20 GPa applying conjugate gradient method to the system. In order to find symmetries of the phases observed in the simulations, we used the RGS algorithm and the KPLOT program [24, 25] that permitted detailed data about a given structure such as space group, cell parameters, and atomic positions.

*corresponding author; e-mail: ckurkcu@ahievran.edu.tr

The relative stability of the different phases of CrO_2 under finite pressure and temperature can be easily identified by a simple comparison of their Gibbs free energies, $G = E_{\rm tot} + PV - TS$. Since calculations in this study are achieved at zero temperature, the last term is ignored. As a result, the static enthalpy can be expressed as $H = E_{\rm tot} + PV$, where pressure is acquired by direct differentiation of the energy-volume curves i.e., $P = -{\rm d}E_{\rm tot}/{\rm d}V$ [26]. The rutile-type, $CaCl_2$-type and orthorhombic structures were equilibrated at several volumes and their energy-volume relations were fitted to the third-order Birch–Murnaghan equation of state [27, 28]. For the energy–volume calculations, the Brillouin zone integration was achieved with an automatically created 6-6-6 k-point mesh for three phases of CrO_2 succeeding the convention of Monkhorst and Pack [29]. Enthalpy calculations supply generally accurate transition pressures comparable to experiments. These pressures can be easily found by matching the enthalpy of the phases for the reason that the phase transitions emerge at equal enthalpy of the two phases transformed one to another one.

3. Results and discussions

Initially, we relax a 96 atoms supercell at zero pressure to obtain the lattice parameters of the $P4_2/mnm$ phase and afterwards compare them with available literature data. The equilibrium unit cell lattice constants of CrO_2 are obtained as $a = 4.3754$ Å, and $c/a = 0.5927$. These values are comparable with the previous experimental results of $a = 4.4190$–4.4320 Å and $c/a = 0.6568$–0.6597 [12, 16, 19, 21] and the theoretical results of $a = 4.3840$–4.4560 Å and $c/a = 0.6349$–0.6597 [18, 30, 31].

The pressure–volume relation of CrO_2 is investigated and presented in Fig. 1. The volume gives sharp variations when the applied pressure is increased from 200 GPa to 220 GPa, and from 420 GPa to 440 GPa indicating pressure-induced phase transitions in this material. The structural analysis reveals that the tetragonal rutile-type structure transforms to the orthorhombic $CaCl_2$-type structure at 220 GPa and this $CaCl_2$-type structure transforms to another orthorhombic structure at 440 GPa, as shown in Fig. 2. Their equilibrium lattice parameters and the atomic fractional coordinates are summarized in Table I. In order to examine whether there are another phase transformations or not, we have increased the pressure up to 500 GPa. We have not observed any other phase for CrO_2.

The obtained phase transition pressure values using gradually increasing pressure technique show that the *ab initio* technique successfully produces the experimentally observed high-pressure phase of CrO_2 with an overvalued transition pressure. Since the restricted conditions such as finite size of the simulation cell, the lack of any defect in simulated structure, etc. are considered,

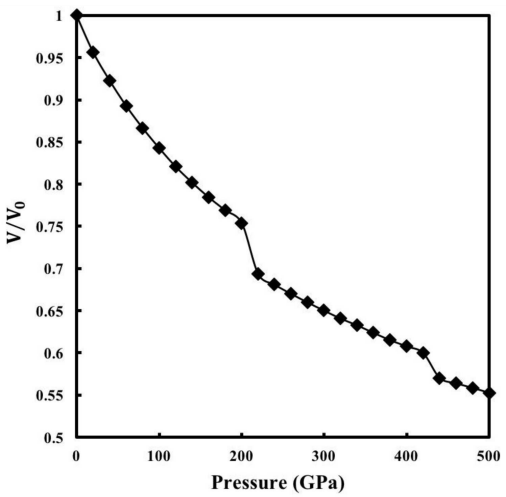

Fig. 1. The volume change of the simulation cell as function of pressure.

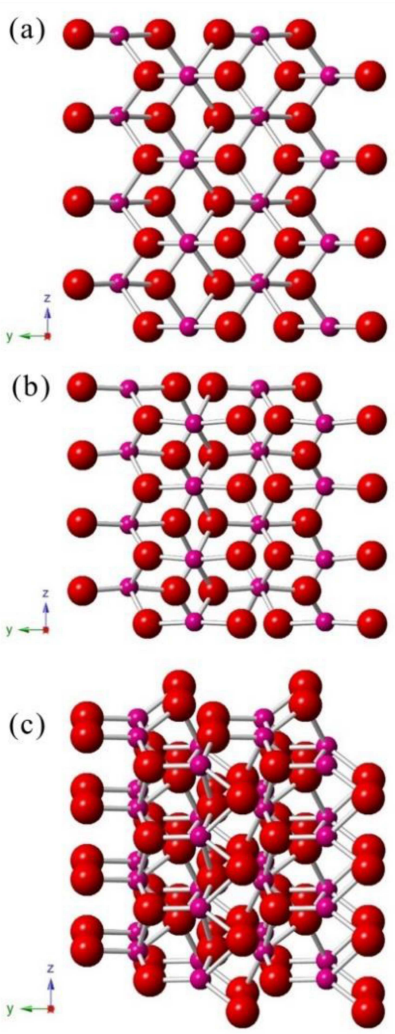

Fig. 2. Crystal structures of CrO_2: (a) $P4_2/mnm$ at zero pressure, (b) $Pnnm$ at 220 GPa, and (c) $Cmc2_1$ at 440 GPa.

TABLE I

Equilibrium lattice parameters and atomic fractional coordinates of three main phases of CrO_2

Phase	a [Å]	b [Å]	c [Å]	x	y	z
$P4_2/mnm$	4.3754	4.3754	2.5932	Cr: 0.5000	0.5000	0.5000
				O: 0.7890	0.7890	0.5000
				O: 0.2110	0.2110	0.5000
$Pnnm$	3.7145	4.2312	2.1888	Cr: 0.5000	0.5000	0.5000
				O: 0.3136	0.1437	0.5000
				O: 0.6864	0.8563	0.5000
$Cmc2_1$	2.0887	7.4108	3.6589	Cr: 0.0000	0.3813	0.0001
				O: 0.0000	0.9548	0.6684
				O: 0.5000	0.4548	0.6684

TABLE II

Transition pressures, equilibrium lattice parameters, equilibrium volume rates, bulk modulus and their pressure derivatives of three main phases of CrO_2.

Phase	Pressure [GPa]	a [Å]	b [Å]	c [Å]	V [Å^3]	B_0 [GPa]	B_0'	Reference
$P4_2/mnm$	0	4.3754	4.3754	2.5932	49.65	344	4.39	this study
		4.4210	4.4210	2.9160	56.990	235±10	5 ± 2	[12] (exp.)
		4.4190	4.4190	2.9120				[16] (exp.)
						238	4.4	[17] (exp.)
		4.3840	4.3840	2.8890	55.53	143.3		[18]
		4.4190	4.4190	2.9150	56.923	280±20		[19] (exp.)
		4.4320	4.4320	2.9200		225		[21] (exp.)
		4.4190	4.4190	2.9154	56.930			[30]
		4.4560	4.4560	2.8290	56.17	282.47	4.57	[31]
$Pnnm$	15	3.7145	4.2312	2.1888	34.40	308.82	4.27	this study
	12±3	4.3874	4.2818	2.8779	58.01 ± 0.1	162±2	4	[12] (exp.)
						202	3.7	[17] (exp.)
	9.6	4.3540	4.2490	2.8580		193		[18]
	14	4.3930	4.2910	2.8810		234		[21] (exp.)
	10.9				56.63	179.33	4.31	[31]
$Cmc2_1$	105	2.0887	7.4108	3.6589	56.63	272.47	4.58	this study

such an overestimated transition pressure is expected [32]. Conversely, the thermodynamic theorem does not take into account the probable presence of an activation barrier separating the two structural phases. Thus, as a next step, we take the energy–volume computations into account to study the stability of high-pressure phases of CrO_2. For these computations we used the unit cells for the $P4_2/mnm$, $Pnnm$, and $Cmc2_1$ high-pressure phases. Both of the unit cells of the first two phases have 6 atoms and the unit cell of the last phase has 12 atoms.

The third-order Birch–Murnaghan equation of state, given by

$$P = 1.5B_0 \left[\left(\frac{V}{V_0} \right)^{-\frac{7}{3}} - \left(\frac{V}{V_0} \right)^{-\frac{5}{3}} \right] \times \left\{ 1 + 0.75 \left(B_0' - 4 \right) \left[\left(\frac{V}{V_0} \right)^{-\frac{2}{3}} - 1 \right] \right\}, \quad (1)$$

was used to fit the energy–volume data for three main structures of CrO_2. Here P is the pressure, V is the volume at pressure, V_0, B_0, and B_0' are the volume, bulk modulus, and its first pressure derivate at 0 GPa, respectively [27, 28]. The computed total energies as a function of volumes are presented in Fig. 3. The equilibrium lattice parameters, equilibrium volume rates, bulk modulus, and their pressure derivatives, together with the other theoretical and experimental data for three main structures of CrO_2 are reported in Table II. The bond lengths between Cr and O atoms with minimum and maximum values and coordination numbers of the $P4_2/mnm$, $P\bar{4}2_1m$, $P2_12_12$, $Pnnm$, $P2_1/c$, $P2_1$, and $Cmc2_1$ phases are given in Table III and the calculated density and porosity data of these phases are given in Table IV.

The phase transition pressure between different phases of CrO_2 is easily identified by a simple comparison of their static lattice enthalpy since the intersection of two enthalpy curves indicates a pressure-induced phase

transition between these two phases. The computed enthalpy curves of the $P4_2/mnm$, $Pnnm$, and $Cmc2_1$ high-pressure phases are plotted as a function of pressure in Fig. 4. As seen from this figure the enthalpy curve of the $P4_2/mnm$ phase crosses with that of the $Pnnm$ phase at about 15 GPa indicating phase transition between these phases and the enthalpy curve of the $Pnnm$ phase crosses with that of the $Cmc2_1$ phase at about 105 GPa between these phase couple indicating another phase transition.

In order to evaluate transformation mechanism at the atomistic level, we investigate the variations of the simulation cell vectors and angles as a function of minimization step. Figure 5 displays the modification of the simulation cell lengths and angles at 220 and 440 GPa, respectively. These simulation cell vectors are called as $\boldsymbol{A}$, $\boldsymbol{B}$, and $\boldsymbol{C}$ which are initially along the [100], [010], and [001] directions, respectively.

TABLE III

The bond lengths with minimum and maximum values and coordination numbers of the $P4_2/mnm$, $P\bar{4}2_1m$, $P2_12_12$, $Pnnm$, $P2_1/c$, $P2_1$ and $Cmc2_1$ phases. $B_{\min}$ and $B_{\max}$ indicate minimum and maximum bond lengths, respectively.

Phase	$B_{\min}$ [Å]	$B_{\max}$ [Å]	Coordination
$P4_2/mnm$	1.773	1.863	Cr $\Longrightarrow$ [2–6]O
			O $\Longrightarrow$ [1–3]Cr
$P\bar{4}2_1m$	1.571	1.722	Cr $\Longrightarrow$ [2–6]O
			O $\Longrightarrow$ [1–3]Cr
$P2_12_12$	1.580	1.763	Cr $\Longrightarrow$ [2–6]O
			O $\Longrightarrow$ [1–3]Cr
$Pnnm$	1.641	1.743	Cr $\Longrightarrow$ [2–6]O
			O $\Longrightarrow$ [1–3]Cr
$P2_1/c$	1.565	1.702	Cr $\Longrightarrow$ [2–6]O
			O $\Longrightarrow$ [1–3]Cr
$P2_1$	1.565	2.164	Cr $\Longrightarrow$ [2–7]O
			O $\Longrightarrow$ [1–4]Cr
$Cmc2_1$	1.615	1.725	Cr $\Longrightarrow$ [2–7]O
			O $\Longrightarrow$ [1–4]Cr

TABLE IV

The calculated density and porosity data of the $P4_2/mnm$, $P\bar{4}2_1m$, $P2_12_12$, $Pnnm$, $P2_1/c$, $P2_1$ and $Cmc2_1$ phases.

Phase	Calculated density [kg/m^3]	Unit cell volume [Å^3]	Atom density [atoms/Å^3]	Filled space [Å^3]	Void space [Å^3]
$P4_2/mnm$	1758.7308	2537.9583	0.0378	529.204	2008.754
$P\bar{4}2_1m$	2400.0535	1859.7859	0.0516	509.143	1350.643
$P2_12_12$	2334.0608	1912.3689	0.0502	508.221	1404.148
$Pnnm$	2628.0095	1698.4662	0.0565	504.234	1194.233
$P2_1/c$	2884.3579	1547.5144	0.0620	479.873	1067.642
$P2_1$	2431.8752	1835.4500	0.0523	475.683	1359.767
$Cmc2_1$	2080.3394	2145.6045	0.0447	478.085	1667.520

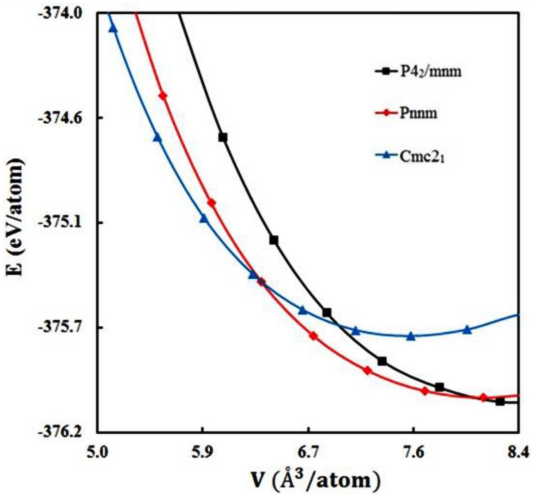

Fig. 3. The energy–volume curves of main structural phases of CrO_2.

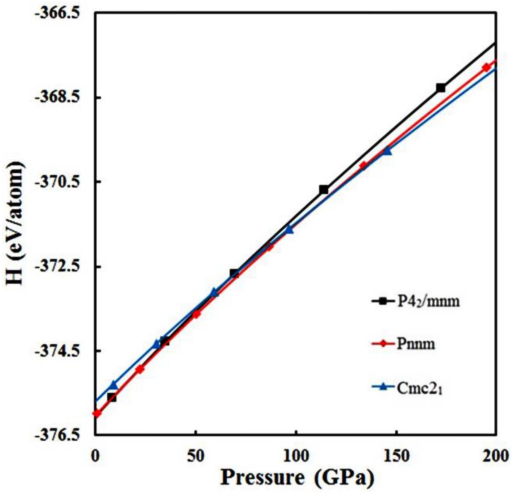

Fig. 4. The enthalpy curves of main structural phases of CrO_2 as function of pressure.

In order to investigate whether there is any intermediate state during the phase transformation or not, we analyzed the obtained structures in this study at each minimization step by using KPLOT program. For the $Pnnm$ phase of CrO_2, we determined a tetragonal structure with $P4_2/mnm$ symmetry at 34$^{\text{th}}$ minimization step and an orthorhombic structure with $P2_12_12$ symmetry at 43$^{\text{rd}}$ minimization step. The orthorhombic $CaCl_2$-type structure having $Pnnm$ symmetry forms at 71$^{\text{st}}$ minimization step. These intermediate states are depicted in Fig. 6. For the $Cmc2_1$ phase of CrO_2, we observed a monoclinic structure with $P2_1/c$ symmetry at 33$^{\text{rd}}$ minimization step and another monoclinic structure with $P2_1$ symmetry at 99$^{\text{th}}$ minimization step. The orthorhombic structure having $Cmc2_1$ symmetry forms at 130$^{\text{th}}$ minimization step. These intermediary states are depicted in Fig. 7.

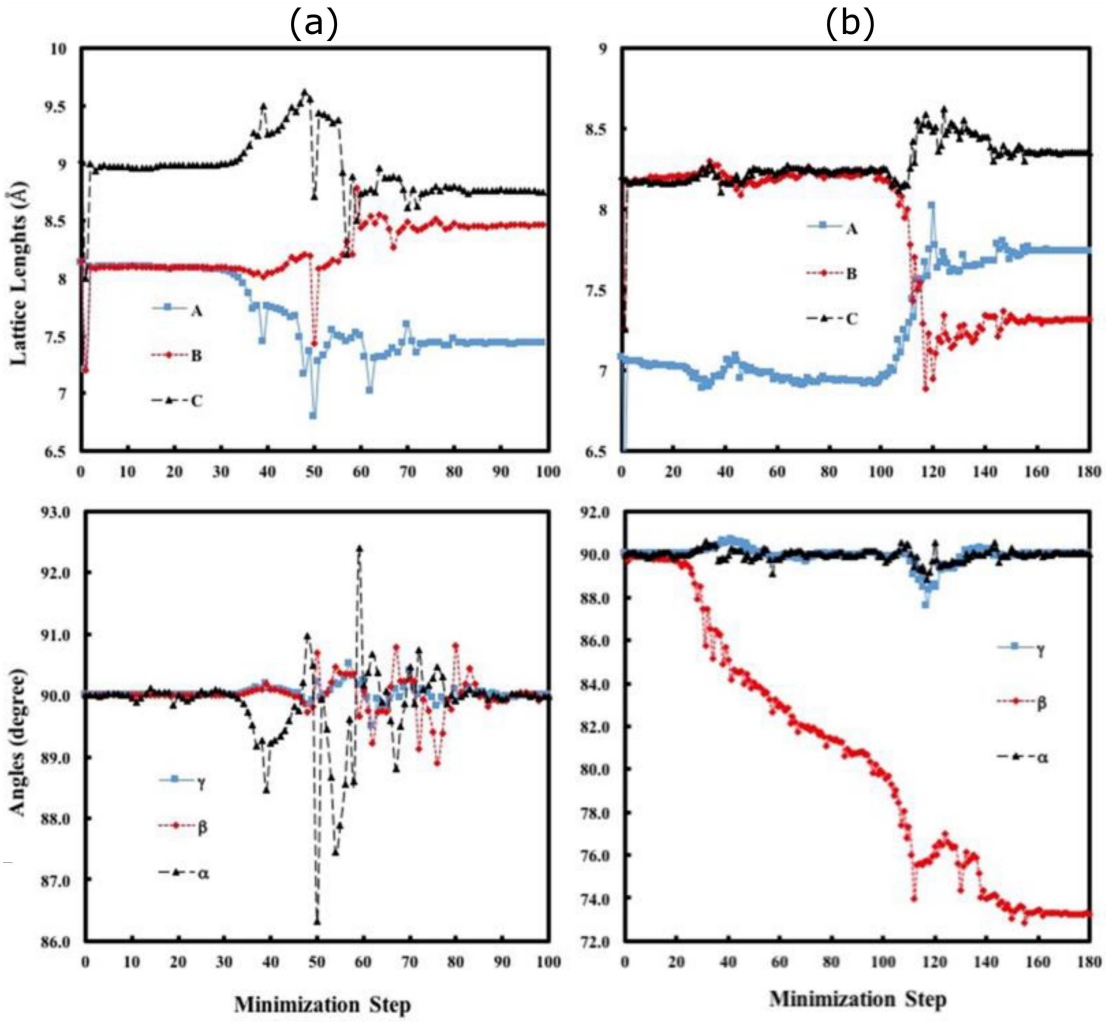

Fig. 5. The behavior of the simulation cell lengths and angles as function of minimization steps: (a) at 220 GPa and (b) at 440 GPa.

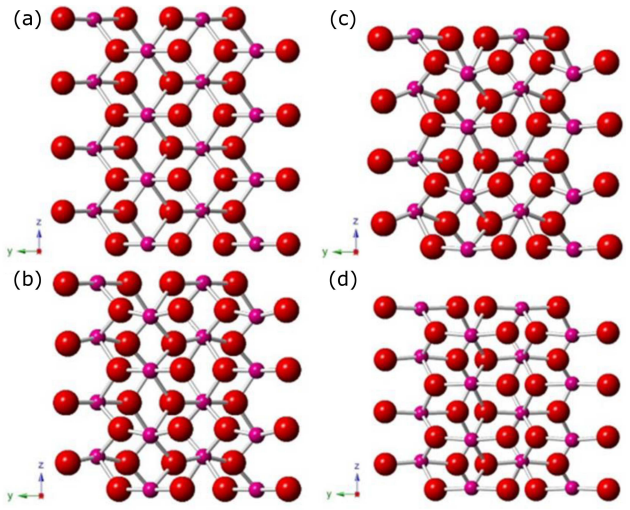

Fig. 6. Evolution of the $Pnnm$ phase at 220 GPa: (a) $P4_2/mnm$, (b) $P\bar{4}2_1m$, (c) $P2_12_12$, and (d) $Pnnm$.

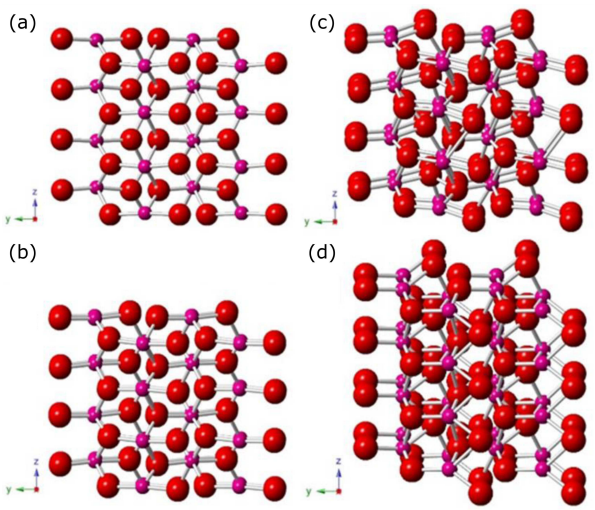

Fig. 7. Evolution of the $Cmc2_1$ phase at 440 GPa: (a) $Pnnm$, (b) $P2_1c$, (c) $P2_1$, and (d) $Cmc2_1$.

We calculated the band structures with minority and majority spin states along the high-symmetry directions for $P4_2/mnm$, $Pnnm$, and $Cmc2_1$ phases of CrO_2. Figures 8–10 illustrate band structures of main phases of CrO_2 near the Fermi energy (E_F) level at 0 GPa, 220 GPa and 440 GPa pressure, respectively. The Fermi levels were set to be 0 eV. The symmetry points were $\Gamma, X, M, \Gamma, Z, R, A$, and M for $P4_2/mnm$ phase, $\Gamma, Z, T, Y, \Gamma, X, S, R$, and U for $Pnnm$ phase, and $\Gamma, Z, T, Y, \Gamma, S, R$, and Z for $Cmc2_1$ phase. In Fig. 8, the electronic band curves for the spin up state show that $P42/mnm$ phase of CrO_2 has metallic character. In the event of spin down state, there is a direct band gap because the valence band maximum and conduction band minimum are situated at the same point (Γ-point). Since the band curves obtained for spin up and spin down states do not overlap, the $P4_2/mnm$ phase of CrO_2 also has a magnetic property. In Fig. 9, according to the obtained band curves, it is obvious that the $Pnnm$ phase of CrO_2 has metallic properties as they cut the Fermi level. In Fig. 10, $Cmc2_1$ phase of CrO_2 is similar to the semiconductor character having a direct band gap at S-point. However, since the band curves for the spin up and spin down states overlap, the $Pnnm$ and $Cmc2_1$ phases of CrO_2 do not have magnetic properties.

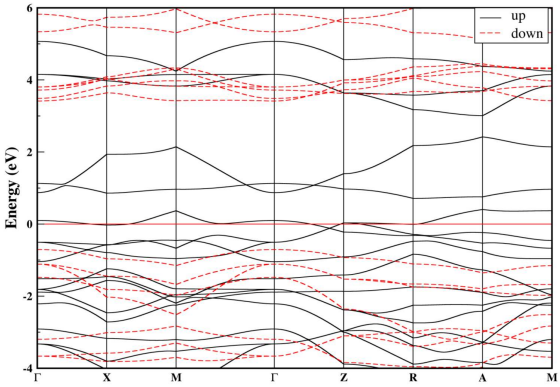

Fig. 8. The calculated spin polarized band structures of CrO_2 at 0 GPa.

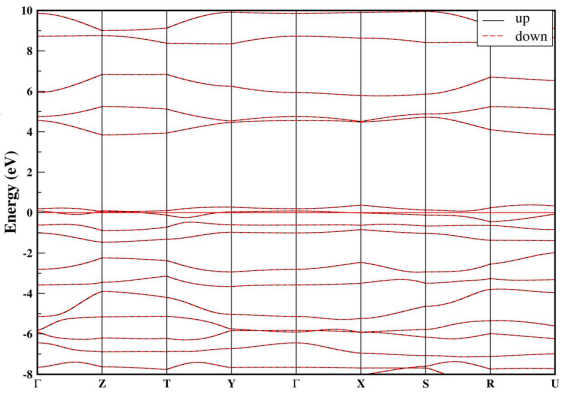

Fig. 9. The calculated spin polarized band structures of CrO_2 at 220 GPa.

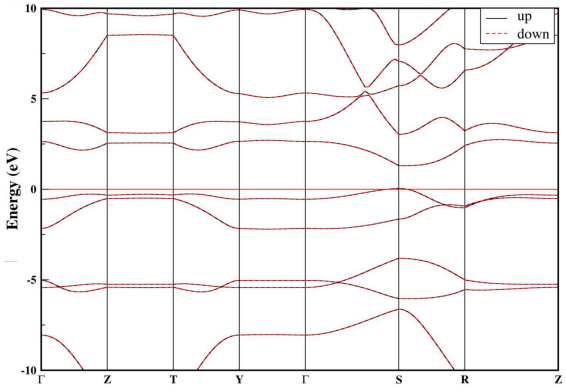

Fig. 10. The calculated spin polarized band structures of CrO_2 at 440 GPa.

4. Conclusions

We have performed an *ab initio* constant pressure technique in order to study the pressure-induced phase transformation in the rutile-type structured chromium dioxide. The phase transition path is obtained as $P4_2/mnm \rightarrow Pnnm \rightarrow Cmc2_1$. Two intermediary states are observed for both phase transitions. These intermediary states and the orthorhombic structure with space group $Cmc2_1$ of CrO_2 have not been observed in any other previous studies to our knowledge. Additionally, we calculated the electronic band structure of CrO_2. From these calculations, it can be seen that all phases have metallic character. In addition, the $P4_2/mnm$ phase of CrO_2 shows a magnetic property while the other high pressure phases do not have magnetic properties. Our findings allow different viewpoints on the transformation mechanism of the rutile-type structure to the $CaCl_2$-type structure phase change and that of $CaCl_2$-type structure to the orthorhombic structure with space group $Cmc2_1$.

Acknowledgments

This study was supported by the Ahi Evran University Scientific Research Projects Coordination Unit. Project Number: FEF.A3.16.026.

References

[1] Y. Ji, G.J. Strijkers, F.Y. Yang, C.L. Chien, J.M. Byers, A. Anguelouch, G. Xiao, A. Gupta, *Phys. Rev. Lett.* **86**, 5585 (2001).

[2] J.S. Parker, S.M. Watts, P.G. Ivanov, P. Xiong, *Phys. Rev. Lett.* **88**, 196601 (2002).

[3] K.P. Kämper, W. Schmitt, G. Güntherodt, R.J. Gambino, R. Ruf, *Phys. Rev. Lett.* **59**, 2788 (1987).

[4] Y.S. Dedkov, M. Fonin, C. König, U. Rüdiger, G. Güntherodt, S. Senz, D. Hesse, *Appl. Phys. Lett.* **80**, 4181 (2002).

[5] J.M.D. Coey, A.E. Berkowitz, L.I. Balcells, F.F. Putris, A. Barry, *Phys. Rev. Lett.* **80**, 3815 (1998).

[6] J.M.D. Coey, S. Sanvito, *J. Phys. D Appl. Phys.* **37**, 988 (2004).

[7] D.J. Huang, L.H. Tjeng, J. Chen, C.F. Chang, W.P. Wu, S.C. Chung, A. Tanaka, G.Y. Guo, H-J. Lin, S.G. Shyu, *Phys. Rev. B* **67**, 214419 (2003).

[8] C.B. Stagarescu, X. Su, D.E. Eastman, K.N. Altmann, F.J. Himpsel, A. Gupta, *Phys. Rev. B* **61**, R9233 (2000).

[9] E.Z. Kurmaev, A. Moewes, S.M. Butorin, M.I. Katsnelson, L.D. Finkelstein, J. Nordgren, P.M. Tedrow, *Phys. Rev. B* **67**, 155105 (2003).

[10] M.N. Iliev, A.P. Litvinchuk, H.G. Lee, C.W. Chu, A. Barry, J.M.D. Coey, *Phys. Rev. B* **60**, 33 (1999).

[11] K. Schwarz, *J. Phys. F Met. Phys.* **16**, L211 (1986).

[12] B.R. Maddox, C.S. Yoo, D. Kasinathan, W.E. Pickett, R.T. Scalettar, *Phys. Rev. B* **73**, 144111 (2006).

[13] R.M. Hazen, L.W. Finger, *J. Phys. Chem. Solids* **42**, 143 (1981).

[14] J. Haines, J.M. Léger, S. Hoyau, *J. Phys. Chem. Solids* **56**, 965 (1995).

[15] V. Kanchana, G. Vaitheeswaran, M. Alouani, *J. Phys. Condens. Matter* **18**, 5155 (2006).

[16] A.Y. Kuznetsov, J.S. De Almeida, L. Dubrovinsky, R. Ahuja, S.K. Kwon, I. Kantor, A. Kantor, N. Guignot, *J. Appl. Phys.* **99**, 53909 (2006).

[17] V. Srivastava, M. Rajagopalan, S.P. Sanyal, *Europ. Phys. J. B* **61**, 131 (2008).

[18] S.F. Matar, G. Demazeau, *Chem. Phys. Lett.* **407**, 516 (2005).

[19] V.A. Sidorov, A.V. Rakhmanina, O.A. Morya, *Solid State Commun.* **139**, 360 (2006).

[20] Y. Li, J. Hao, *Solid State Commun.* **152**, 1216 (2012).

[21] P.I. Sorantin, K. Schwarz, *Inorg. Chem.* **31**, 567 (1992).

[22] P. Ordejón, E. Artacho, J.M. Soler, *Phys. Rev. B* **53**, R10441 (1996).

[23] D.M. Ceperley, B.J. Alder, *Phys. Rev. Lett.* **45**, 566 (1980).

[24] A. Hannemann, R. Hundt, J.C. Schön, M. Jansen, *J. Appl. Crystallogr.* **31**, 922 (1998).

[25] R. Hundt, J.C. Schön, A. Hannemann, M. Jansen, *J. Appl. Crystallogr.* **32**, 413 (1999).

[26] M. Durandurdu, *J. Phys. Condens. Matter* **20**, 325232 (2008).

[27] F. Birch, *Phys. Rev.* **71**, 809 (1947).

[28] F.D. Murnaghan, *Proc. Natl. Acad. Sci.* **30**, 244 (1944).

[29] H.J. Monkhorst, J.D. Pack, *Phys. Rev. B* **13**, 5188 (1976).

[30] H.Y. Wu, Y.H. Chen, C.R. Deng, X.F. Su, *Phase Transit.* **85**, 708 (2012).

[31] S. Alptekin, *J. Mol. Model.* **21**, 1 (2015).

[32] R. Martoňák, A. Laio, M. Parrinello, *Phys. Rev. Lett.* **90**, 075503 (2003).